Linear and nonlinear convection in porous media between coaxial cylinders

Carina Bringedal,[1,a)] Inga Berre,[1] Jan M. Nordbotten,[1] and D. Andrew S. Rees[2]
[1]*Department of Mathematics, University of Bergen, 5020 Bergen, Norway*
[2]*Department of Mechanical Engineering, University of Bath, Bath BA2 7AY, United Kingdom*

(Received 2 May 2011; accepted 18 August 2011; published online 16 September 2011)

We uncover novel features of three-dimensional natural convection in porous media by investigating convection in an annular porous cavity contained between two vertical coaxial cylinders. The investigations are made using a linear stability analysis, together with high-order numerical simulations using pseudospectral methods to model the nonlinear regime. The onset of convection cells and their preferred planform are studied, and the stability of the modes with respect to different types of perturbation is investigated. We also examine how variations in the Rayleigh number affect the convection modes and their stability regimes. Compared with previously published data, we show how the problem inherits an increased complexity regarding which modes will be obtained. Some stable secondary modes or mixed modes have been identified and some overlapping stability regions for different convective modes are determined. © *2011 American Institute of Physics*. [doi:10.1063/1.3637642]

I. INTRODUCTION

Describing fluid flow and transport phenomena in a porous medium is a widely investigated topic. Bear[1] gives a thorough introduction to fluid dynamics in porous media, while the book of Ingham and Pop[2] focuses on the recent research on transport processes in porous media. Modelling transport phenomena in porous media is covered in the book of Bear and Bachmat.[3] Important physical and chemical aspects of our work are relevant for applications in groundwater flow such as geothermal energy extraction (see, e.g., Freeze and Cherry).[4]

Various aspects of natural convection in porous media have been investigated in the last half century. The critical Rayleigh number for the onset of natural convection in a uniform horizontal porous layer of infinite extent which is heated from below was determined to be $4\pi^2$ by Horton and Rogers[5] and later Lapwood.[6] Horton, Rogers, and Lapwood confined their interest to cases where the upper and lower surfaces are impermeable and perfectly heat conducting, while later work, such as the paper by Nield,[7] also investigated permeable upper and lower surfaces subject to constant heat fluxes. A table showing how the critical Rayleigh number and the corresponding wavenumber depend on the type of boundary condition which has been applied may be found in Nield and Bejan.[8]

Later works have included enquiries concerning geometries other than horizontally infinite cavities; Beck[9] investigated the case of a finite cuboidal box with insulated and impermeable lateral walls together with perfectly conducting horizontal surfaces. A very similar paper by Wang[10] studies a lower surface subject to a constant heat flux, whilst the upper surface remains perfectly conducting. A circular cylinder with impermeable walls and insulated sidewalls was considered by Zebib,[11] and Wang[12] solved the same problem as Zebib but subjected the upper surface to constant temperature and pressure boundary conditions while the lower surface was impermeable but could be held either at a constant temperature or at a constant heat flux. These last two authors presented mode maps in the style of Beck.[9] The case of a circular cylinder with perfectly conducting boundaries was considered by Haugen and Tyvand,[13] who also compared their findings with Zebib's results. In the papers concerning convection in cylinders, the criterion for the onset of convection is given as a function of the radius of the vertical outer boundary. An annular cylindrical cavity with insulated sidewalls was investigated by Bau and Torrance.[14] They allowed the upper surface to be either permeable or impermeable and found criteria for the onset of convection and preferred mode shapes as functions of the inner and outer radii of the cavity.

The analytical part of this paper is related to the paper of Bau and Torrance.[14] Using linear stability analysis, we will determine the criterion for the onset of convection and the corresponding preferred convective mode for an annular cylinder having impermeable walls. While Bau and Torrance only considered insulated sidewalls, we will extend their work and also allow for conducting sidewalls. The two different cases are also compared.

We will also present the results of investigations of the nonlinear time-dependent equations using an unsteady 3D-simulator based on pseudospectral methods. The simulator allows us to determine how far into the nonlinear regime the onset mode found using the linear theory persists as the favored mode. We are also able to determine whether secondary modes or mixed modes become possible stable nonlinear solutions.

The outline of this paper is as follows: We begin by presenting the governing, nonlinear equations and define the domain together with boundary conditions in Sec. II. In Sec. III, we perform a linear stability analysis on the governing equations; conditions for the onset of convection as well as preferred convective modes are determined. In Sec. IV, we

[a)]Electronic mail: carina.bringedal@student.uib.no.

perform some exploratory investigations of the nonlinear regime by means of a suitable unsteady solver for the original nonlinear equations. Finally, conclusions are made in Sec. V.

II. MATHEMATICAL FORMULATION

A cylinder with an annular planform height, h^*, inner radius, R_w^*, and outer radius, R^*, is filled with a porous medium (see Figure 1). The porous medium is isotropic and homogeneous, and it is assumed that the fluid and solid phases are in local thermal equilibrium. All the bounding surfaces of the cylinder, both vertical and horizontal, are impermeable. The upper and lower surfaces are taken to be perfectly heat conducting and are kept at the constant temperatures T_c^* and T_h^*, respectively. The cylinder is heated from below and cooled from above; hence, T_c^* is smaller than T_h^*. The vertical sidewalls are either insulated or conducting, meaning that there is either no heat flow over the sidewalls or it is kept at a steady temperature which decreases linearly with z from T_h^* to T_c^*. Thus, we consider two cases, namely, that either both sidewalls are insulated or both sidewalls are perfectly conducting.

The dimensionless Darcy-Boussinesq equations for convection in a homogeneous and isotropic porous medium are given by

$$\mathbf{v} = -\nabla P + \mathrm{Ra} T \mathbf{k}, \psi \tag{1}$$

$$\nabla \cdot \mathbf{v} = 0, \psi \tag{2}$$

$$\frac{\partial T}{\partial t} + \mathbf{v} \cdot \nabla T = \nabla^2 T, \psi \tag{3}$$

where the dimensionless Rayleigh number Ra is given by

$$\mathrm{Ra} = \frac{gK\beta h^* \Delta T^*}{\nu \alpha}. \psi \tag{4}$$

In the above equation, g is gravity, K is permeability, β is the thermal expansion coefficient of the saturating fluid, $\Delta T^* = T_h^* - T_c^*$ is the temperature difference between the top and bottom of the cylinder, ν is the kinematic viscosity,

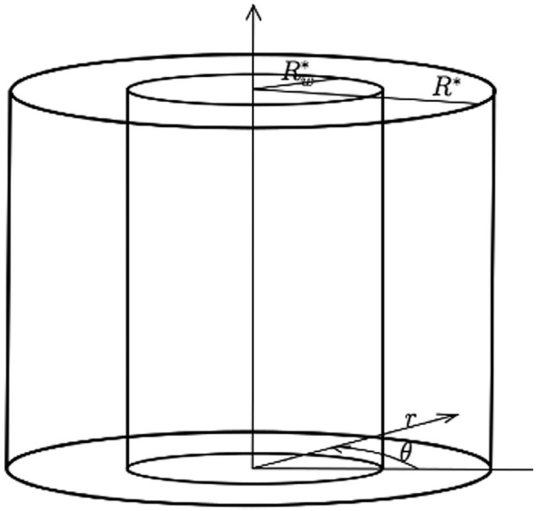

FIG. 1. Sketch of the annular cylindrical configuration.

and α the thermal diffusivity of the fluid. In Eqs. (1)–(3), $\mathbf{k}$ is a unit vector pointing upwards, $\mathbf{v}$ is the fluid velocity, P is pressure, and T is temperature. The last three quantities are all nondimensional variables. Cylindrical coordinates are used; hence, the fluid velocity is the vector $\mathbf{v} = v_r \mathbf{e}_r + v_\theta \mathbf{e}_\theta + v_z \mathbf{k}$, where $\mathbf{e}_r$ and $\mathbf{e}_\theta$ are unit vectors in the radial and the azimuthal direction, respectively.

In nondimensional terms, the cylinder has height 1, inner radius $R_w = R_w^*/h^*$, and outer radius $R = R^*/h^*$. The boundary conditions associated with Eqs. (1)–(3) are impermeable sidewalls,

$$v_r = 0 \text{ at } r \in \{R_w, R\}, \psi$$

together with the top and bottom of the cylinder being impermeable and perfectly heat conducting. The lower surface is heated and the upper surface is cooled, modeled by the boundary conditions,

$$T = 1 \text{ and } v_z = 0 \text{ at } z = 0, \psi$$

$$T = 0 \text{ and } v_z = 0 \text{ at } z = 1. \psi$$

The thermal boundary conditions on the sidewalls are either

$$\frac{\partial T}{\partial r} = 0 \text{ at } r \in \{R_w, R\}, \psi$$

when the sidewalls are insulated, or

$$T = 1 - z \text{ at } r \in \{R_w, R\}, \psi$$

when the sidewalls are perfectly heat conducting.

III. LINEAR STABILITY ANALYSIS AND MODE MAPS

A better understanding of nonlinear convection is gained by setting it into the context of a linear stability analysis. Configurations which are unbounded horizontally yield neutral stability curves from which the critical Rayleigh number and its corresponding wavenumber may be found. In confined cavities, such as the one considered here, attention is usually focused on the identity of the preferred modal pattern and how it changes as the cavity aspect ratio changes. Therefore, our aim in this section is to solve the three governing equations (1)–(3) by first linearizing them about the basic conduction state.

A. Linearization about the basic state

Equations (1)–(3) together with the above boundary conditions have the steady-state solution,

$$T_s = 1 - z, \psi \qquad \mathbf{v}_s = 0, \psi \qquad P_s = \mathrm{Ra}\left(z - \frac{z^2}{2}\right) + P_0. \psi$$

We now perturb this basic state by adding the small quantities $\hat{T}$, $\hat{\mathbf{v}}$, and $\hat{P}$, respectively. We insert the perturbed expression in the governing equations (1)–(3) and linearize, thereby, obtaining the following equations for the perturbed quantities:

$$\hat{\mathbf{v}} = -\nabla \hat{P} + \mathrm{Ra} \hat{T} \mathbf{k}, \psi \tag{5}$$

$$\nabla \cdot \hat{\mathbf{v}} = 0, \tag{6}$$

$$\frac{\partial \hat{T}}{\partial t} - \hat{v}_z = \nabla^2 \hat{T}. \tag{7}$$

We note that the convective term is the only term to change from the original nonlinear equations (1)–(3).

On assuming that the principle of the exchange of stabilities applies, we neglect the time dependence and combine all three Eqs. (5)–(7) to obtain

$$\nabla^4 \hat{T} + \mathrm{Ra} \nabla_1^2 \hat{T} = 0, \tag{8}$$

where $\nabla_1^2 = \nabla^2 - \frac{\partial^2}{\partial z^2}$. The perfectly conducting boundary condition for the perturbed temperature at the upper and lower surfaces of the cylinder is

$$\hat{T} = 0 \text{ at } z \in \{0, 1\}. \tag{9}$$

The condition of impermeable sidewalls may be rewritten in the form

$$\frac{\partial \psi}{\partial r}(\nabla^2 \hat{T} + \mathrm{Ra}\hat{T}) = 0 \text{ at } r \in \{R_w, R\}, \tag{10}$$

while the fact that the upper and lower surfaces are impermeable leads to the conditions that

$$\nabla^2 \hat{T} = 0 \text{ at } z \in \{0, 1\}. \tag{11}$$

Upon using separation of variables, the general solution of Eq. (8) is a sum of $\hat{T}_1$ and $\hat{T}_2$ given by

$$\hat{T}_1 = [A_m J_m(kr) + B_m Y_m(kr)] \cos(m\theta) \sin(\pi z), \tag{12}$$

$$\hat{T}_2 = \left[C_m J_m\left(\frac{\pi^2}{k} r\right) + D_m Y_m\left(\frac{\pi^2}{k} r\right)\right] \cos(m\theta) \sin(\pi z), \tag{13}$$

when the boundary conditions (9) and (11) have been applied. Here, m is a positive integer, J_m and Y_m are Bessel functions of order m and of the first and second kind, respectively, and k is a wavenumber related to the Rayleigh number through

$$\mathrm{Ra} = \frac{(k^2 + \pi^2)^2}{k^2}. \tag{14}$$

This is identical to the definition of the critical Rayleigh number for rolls in an infinitely large layer when k is identified as being the roll wavenumber. The smallest value of Ra is well known to be $4\pi^2$ when $k = \pi$.

In the above equations, the constants A_m, B_m, C_m, and D_m depend on m and may be found by applying the boundary conditions on the sidewalls, that is, the condition of impermeable sidewalls (10) and the condition of either conducting or insulated sidewalls. These two conditions for the perturbed temperature are either

$$\frac{\partial \hat{T}}{\partial r} = 0 \text{ at } r \in \{R_w, R\}, \tag{15}$$

when the sidewalls are insulated, or

$$\hat{T} = 0 \text{ at } r \in \{R_w, R\}, \tag{16}$$

when the sidewalls are heat conducting.

B. The critical Rayleigh number

If we were to apply the boundary conditions (10) and one of (15) or (16) directly on the perturbed solution $\hat{T}$, we would obtain the zero solution since the four boundary conditions result in four homogenous, linear equations. Nonzero solutions may be obtained by demanding that the determinant of this linear system of equations is zero. On using this approach, we get an eigenvalue problem for the wavenumber k. For the insulated sidewalls, we apply the boundary conditions (10) and (15), and the resulting eigenvalue problem for k may be simplified into the dispersion relation,

$$J_m'(kR_w) Y_m'(kR) - J_m'(kR) Y_m'(kR_w) = 0. \tag{17}$$

For each value of R_w and R, there will be an infinite number of solutions of (17) for each m. We search through all the solutions seeking the wavenumber k_m, which minimizes the Rayleigh number; this provides the critical Rayleigh number for onset of convection,

$$\mathrm{Ra}_c = \min_m \left[\frac{(k_m^2 + \pi^2)^2}{k_m^2}\right]. \tag{18}$$

For the conducting sidewalls case, we use the boundary conditions (10) and (16) and we obtain the dispersion relation,

$$\begin{vmatrix} J_m(kR_w) & Y_m(kR_w) & J_m\left(\frac{\pi^2}{k}R_w\right) & Y_m\left(\frac{\pi^2}{k}R_w\right) \\ J_m'(kR_w) & Y_m'(kR_w) & J_m'\left(\frac{\pi^2}{k}R_w\right) & Y_m'\left(\frac{\pi^2}{k}R_w\right) \\ J_m(kR) & Y_m(kR) & J_m\left(\frac{\pi^2}{k}R\right) & Y_m\left(\frac{\pi^2}{k}R\right) \\ J_m'(kR) & Y_m'(kR) & J_m'\left(\frac{\pi^2}{k}R\right) & Y_m'\left(\frac{\pi^2}{k}R\right) \end{vmatrix} = 0. \tag{19}$$

As for the insulating sidewalls case, our resulting relation has an infinite number of solution and for each R_w and R, we search for the wavenumber k_m which minimizes the Rayleigh number.

For both the conducting and insulated sidewalls cases, and for each value of R_w and R, the critical Rayleigh number is found by minimizing Eq. (18) over the eigenvalues k_m. Hence, we may plot the critical Rayleigh number as a function of R_w and R.

C. Mode maps

For both the conducting and insulated sidewalls cases, it is possible to find the preferred convective mode. Because of the $\cos(m\theta)$ term which appears in Eqs. (12) and (13) for the perturbed temperature, the value of m, which is determined by the minimizing wavenumber k_m, is equal to the number of local maxima (and minima) of the temperature distribution in the azimuthal direction. This temperature distribution corresponds to $2m$ convection cells in the azimuthal direction. For the radial direction, we use the linearized energy equation (7), with the time dependence neglected, to calculate the

radial component of $\hat{v}_z$. If p is the number of sign changes of the radial component of $\hat{v}_z$ in the interval $[R_w, R]$, there are p convection cells in the radial direction. We may, therefore, associate a convective pattern with the numbers (m,p). For each value of R_w and R, a unique preferred convective mode (m,p) can be found for Rayleigh numbers slightly above the critical. Hence, we can plot (m,p) as a function of R_w and R, obtaining a mode map.

Some simple plots may be used to illustrate how mode (m,p) will look in practice. The mode (1,0), which has two adjacent convection cells in the azimuthal direction and no convection cells in the radial direction, will behave as illustrated in Figure 2(a). The mode (0,1) is axisymmetric since $m=0$, and will appear as shown in Figure 2(b). If more convection cells were present in the radial direction, then these would be adjacent. More complex modes will be combinations of the two above, such as in Figure 2(c), which is the convective mode (1,1), and in Figure 2(d), which is (2,1). The plots were made by solving the governing (nonlinear) equations (1)–(3) using pseudospectral methods (see Sec. IV). We applied insulated sidewalls and used a Rayleigh number slightly larger than the critical, hence obtaining the preferred convective mode for various inner and outer radii.

D. Results and discussion

We have found critical Rayleigh numbers and corresponding mode maps for both the insulated and the conducting sidewalls case. In the following, we have limited ourselves to only present results for values of the inner radius ranging from 0 to 2 and the outer radius between 0 and 4.

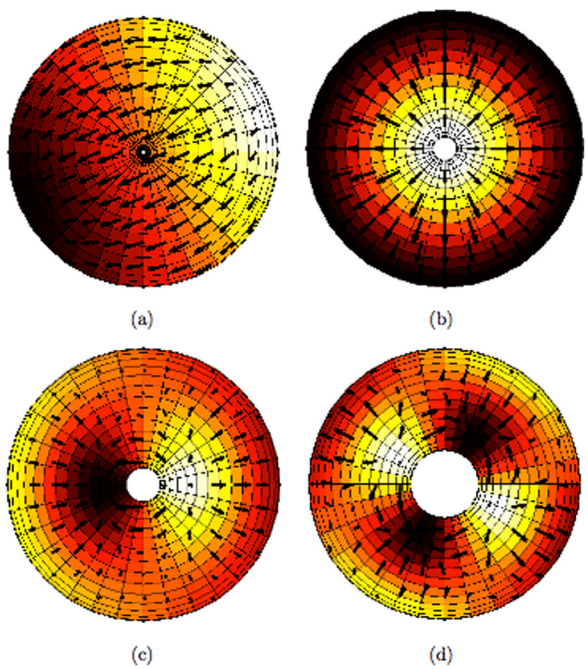

FIG. 2. (Color online) Various simple mode patterns. The shading describes the vertical velocity at $z=0.5$; lighter shades indicate larger, positive velocities, while darker shades indicate larger, negative velocities. The arrows are the radial and azimuthal velocities at $z=1$ seen from above. (a) The mode (1,0) produced using $R_w=0.01$ and $R=0.6$. (b) The mode (0,1) produced using $R_w=0.1$ and $R=1.2$. (c) The mode (1,1) produced using $R_w=0.2$ and $R=1.6$. (d) The mode (2,1) produced using $R_w=0.5$ and $R=2$.

1. Critical Rayleigh number

Critical Rayleigh numbers have been found for both the conducting and insulated sidewall cases. For insulated sidewalls, the function describing the critical Rayleigh number has several local maxima and minima, see Figure 3. The maxima occur when the system goes from one preferred convection mode to another, while the minima, all giving a critical Rayleigh number of $4\pi^2$, occur in between the mode transitions. For increasing values of R, with R_w being held fixed, the critical Rayleigh number will converge towards $4\pi^2$ in the sense that all the local maxima decay towards $4\pi^2$.

Both Zebib[11] (cylinder) and Bau and Torrance[14] (annular cylinder) found the critical Rayleigh number to have several maxima and minima when the sidewalls are insulated. The critical Rayleigh numbers found here are, in general, the same as in the paper of Bau and Torrance, but substantially more values of R_w and R have been considered.

For the conducting sidewall cases, the critical Rayleigh number decreases monotonically as the outer radius R increases, while it increases as the inner radius R_w increases with R held fixed, see Figure 4. For fixed values of R_w, the critical Rayleigh number reduces towards $4\pi^2$ as R increases, but it does so at a slower rate than for the insulated sidewall cases. The small bumps in the contour plot correspond to transitions from one convective mode to another.

Haugen and Tyvand,[13] who considered a circular cylinder of porous medium with a perfectly conducting sidewall, showed that the critical Rayleigh number is a monotonically decreasing function of R and it decreases towards $4\pi^2$ when $R \to \infty$. For fixed nonzero values of R_w, our results are in qualitative agreement. Both Refs. 13, 15 showed that a conducting sidewall does not correspond to a natural cell boundary, and that cells near such a boundary are wider than their insulating sidewall counterparts. Thus, a larger value of R means that an increasing amount of the porous cavity is unaffected by the presence of the boundary. The presence of the inner cylinder does not change this fact and provides a

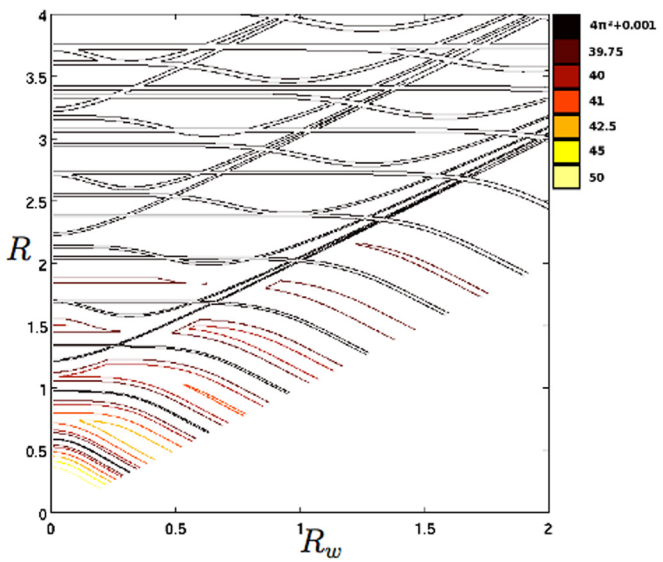

FIG. 3. (Color online) Contour plot of the critical Rayleigh number, Ra_c, as a function of R_w and R when the sidewalls are insulated.

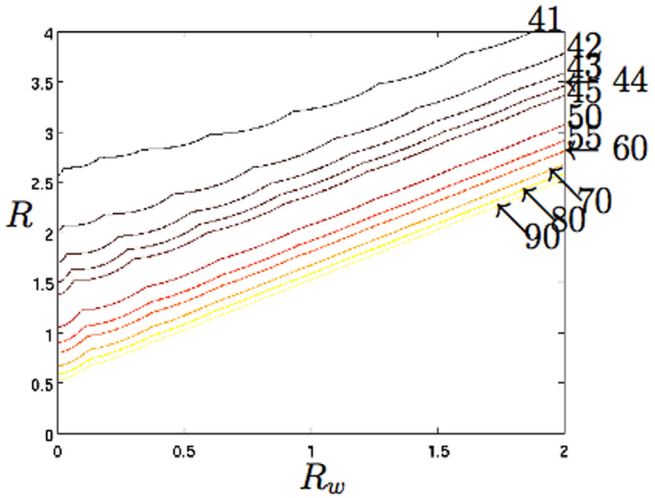

FIG. 4. (Color online) Contour plot of the critical Rayleigh number, Ra_c, for conducting sidewalls.

further restriction to convective flow. When the outer radius, R, is held fixed and the inner radius, R_w, is increased, the critical Rayleigh number increases since the two conducting sidewalls are now closer together, restraining the convection even more. Therefore, it is no surprise that the critical Rayleigh numbers found here for chosen values of the outer radius are always larger than those given by Haugen and Tyvand.

For any choice of values R_w and R, the critical Rayleigh number will be larger for the conducting sidewalls than for the insulated sidewalls. Haugen and Tyvand[13] observed the same for their non-annular cylinder and explained this by conduction being stabilizing as it takes away buoyancy. The presence of an inner cylinder does not change this fact but, instead, we see that a large value of the inner radius increases the critical Rayleigh number even further in the conducting sidewalls case, as more buoyancy is taken away. In the insulated sidewalls case, the effect of an inner cylinder on the critical Rayleigh number is not large. As for the solid cylinder, we observe several maxima and minima related to jumps between different convective modes, but we do not observe a large increase on the critical Rayleigh number when R is fixed and R_w increases.

2. Mode maps

Using the method sketched in Sec. III D 1, the preferred convective mode, (m, p), may be found for both the conducting and insulated sidewall cases. The following mode maps have been produced by finding the values of m and p on a 1000×1000 grid. For insulated sidewalls, we find that a complex pattern forms, which delineates the regions within which different modes are preferred; see Figure 5. The pattern is impossible to describe except in general terms. It is clear that the overall pattern in terms of m has a banded structure where narrow bands exist at certain discrete values of $R - R_w$, which is the width of the annular cavity. When this width is sufficiently small, the number of cells in the azimuthal direction increases as R_w increases, and they also correspond to $p = 0$ implying that the cells have little radial dependence.

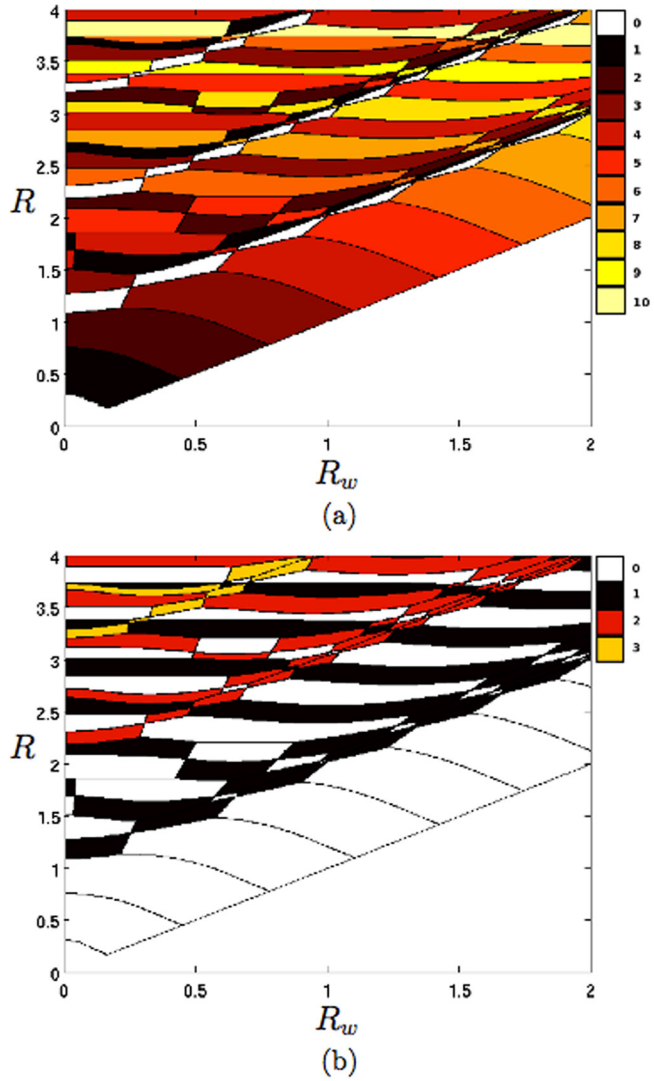

FIG. 5. (Color online) Depiction of the mode maps for insulated sidewalls. (a) The values of m and (b) the values of p.

The values of m and p were also found by Bau and Torrance,[14] and they made a similar mode map with the inner radius on the x-axis and the quotient between the outer and the inner radius on the y-axis. Converting our plot in the same manner enables us to compare our mode map with the one made by Bau and Torrance; see Figure 6. Note that the notation of Bau and Torrance is slightly different from ours; their mode (m,p) corresponds to $(m,p-1)$ in our notation. We have, in general, found the same modes as Bau and Torrance; hence, we have not named our modes in the figure. We find more details in the mode map than Bau and Torrance, and simulations confirm these results. Bau and Torrance do not explain in detail how they obtained their mode map, but we can conclude that their method was not able to produce a sufficiently detailed mode map in some regions. Bau and Torrance concluded that the preferred convection modes are predominantly asymmetric; that is, m is nonzero. In our study, we also find m to be nonzero in general, but several axisymmetric convection modes are found. Hence, we

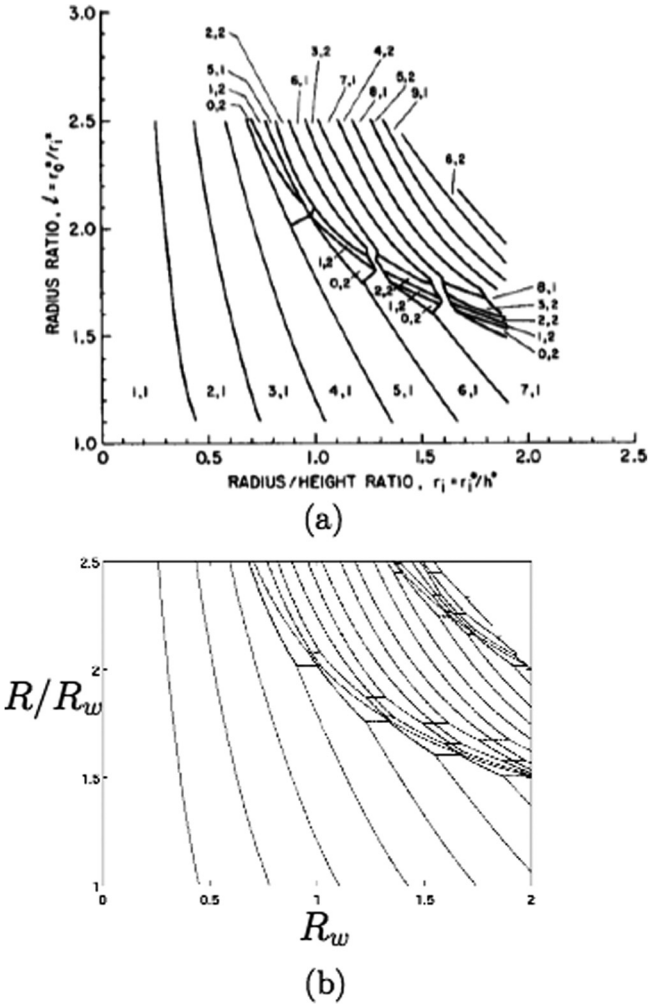

FIG. 6. Comparison between the mode map of Bau and Torrance, and that of the present analysis for insulating sidewalls. (a) The mode map made by Bau and Torrance and is a copy of Figure 3 in Ref. 14. (b) Our version of the Bau and Torrance mode map. Reprinted with permission from H. H. Bau and K. E. Torrance, Phys. Fluids **24**(3), 382 (1981). Copyright 1981, American Institute of Physics.

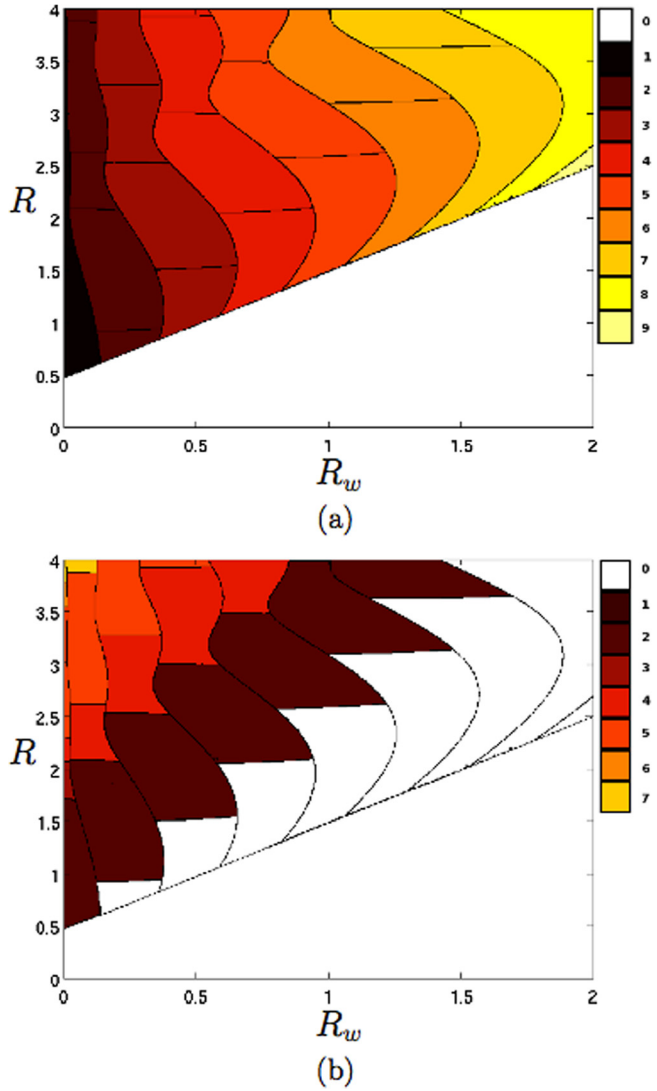

FIG. 7. (Color online) Depiction of the mode maps for conducting sidewalls. (a) The values of m and (b) the values of p.

cannot support Bau and Torrance's conclusion of preferred modes being predominantly asymmetric.

For conducting sidewalls, the overall structure of the mode map is much more structured. We see that the value of m increases as the inner radius R_w is increased and the outer radius R is held fixed; see Figure 7. Although not visible in the figure, m will become zero when R_w is smaller than 10^{-4}. The value of p is zero when the outer radius is not much larger than the inner radius, while for larger values of R, we get larger values of p.

An increasing value of m for increasing R_w means that we get more convection cells in the azimuthal direction for a larger inner radius. This is reasonable since, for R held fixed, an increasing R_w means that the porous medium is getting more narrow, and it is more convenient for the fluid to flow in the azimuthal direction than in the radial since the closeness of the inner and outer sidewalls takes away buoyancy. Also, it is hard for the convection cells to stretch around the inner radius of the cylinder; hence, we get many small convection cells instead of a few large. The increase of p for increasing R can be explained in a similar manner; when the outer radius is not much larger than the inner radius, the narrowness of the porous media makes it difficult for convection cells in the radial direction to occur. Hence, a wider porous medium encourages convection cells in the radial direction to appear.

This far, we have concentrated only on primary modes, i.e., those which minimize the Rayleigh number, but higher modes also exist and these have to be computed as part of the minimization procedure for Ra. For any positive integer n, we denote the nth order Rayleigh numbers by $\mathrm{Ra}_{c,n}$, where $\mathrm{Ra}_{c,1}$ is the overall critical Rayleigh number. We note that, for both conducting and insulated sidewalls, these higher order Rayleigh numbers which are larger than the critical Rayleigh number also vary with R and R_w, but they converge towards $4\pi^2$ at the same rate as in the same speed as for the primary mode. $\mathrm{Ra}_{c,n}$ will be equal to $\mathrm{Ra}_{c,n+1}$ at the bifurcation trajectories in the mode map for (m_n, p_n). For increasing R, this occurs more frequently, meaning that higher order modes are clustered.

3. The limiting case when R_w goes to zero

Zebib[11] and Haugen and Tyvand[13] undertook linear stability analyses similar to ours for a circular (rather than an

annular) cylinder. Their cylinders had insulated and heat conducting sidewalls, respectively. In our eigenvalue problems, the dispersion relations given by Eqs. (17) and (19) may be studied in the limit as the inner radius approaches zero in order to determine if our problem reduces to those of Zebib and of Haugen and Tyvand.

Letting the inner radius approach zero in Eqs. (17) and (19) is not straightforward since the Bessel functions of second kind, Y_m, are singular at zero. The function $Y_m(x)$ behaves as $O(x^{-m})$ as $x \to 0$, except for $Y_0(x)$ which behaves as $O(\ln(x))$. The derivatives $Y'_m(x)$ behave as $O(x^{-m-1})$. On the other hand, Bessel functions of the first kind are nonsingular and have nonsingular derivatives at zero. Letting R_w approach zero in Eq. (17) will cause the second term, $J'_m(kR)Y'_m(kR_w)$ to dominate the equation; hence, we need

$$J'_m(kR) = 0, \psi \tag{20}$$

which is the same equation obtained by Zebib. We can apply a first order Taylor series expansion to Eq. (17) around $k = k^0 + O(R_w^{2m})$ when $m \neq 0$ and around $k = k^0 + O(R_w^2)$ when $m = 0$ as R_w approaches zero. Here, k^0 are the corresponding wavenumbers found by Zebib and k are the wavenumbers found by us using a small value of R_w. This approach will balance all terms in Eq. (17), hence implying that $\mathrm{Ra}_c = \mathrm{Ra}_c^0 + O(R_w^{2m})$ when $m \neq 0$ and $\mathrm{Ra}_c = \mathrm{Ra}_c^0 + O(R_w^2)$ when $m = 0$. Here, Ra_c^0 are the critical Rayleigh numbers found by Zebib for a non-annular cylinder. Using $R_w = 10^{-4}$, our critical Rayleigh numbers was approximately the same as the ones found by Zebib, see Figure 8, and we found the same preferred convective modes. Hence, a very small inner radius does not affect the results in a significant manner, and we regard the problems studied by Zebib as a special case of our analysis.

The determinant in Eq. (19) includes a term which involves the factor $\left[Y'_m(kR_w)Y_m\left(\frac{\pi^2}{k}R_w\right) - Y_m(kR_w)Y'_m\left(\frac{\pi^2}{k}R_w\right)\right]$. This term will dominate all the others when R_w approaches zero. Hence, this term must be set to zero, thereby yielding the condition

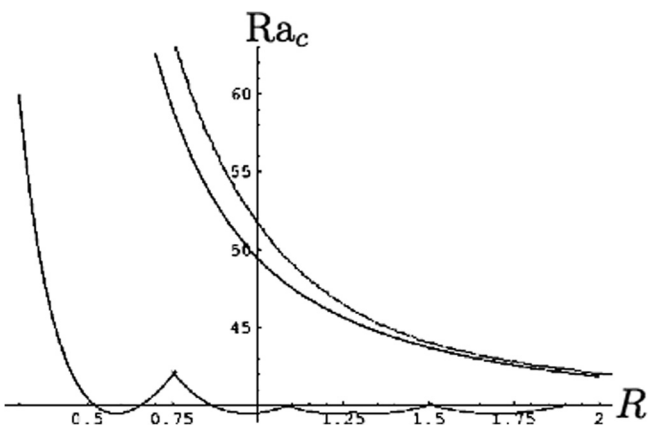

FIG. 8. Variation of Ra_c with R for (i) circular cylinder with an insulated sidewall (Ref. 11, lowest curve), (ii) circular cylinder with a perfectly conducting sidewall (Ref. 13, middle curve), (iii) annular cylinder with perfectly conducting sidewalls and with $R_w = 10^{-4}$. (The figure is adapted from Figure 1 in Ref. 13.)

$$J_m(kR)J'_m\left(\frac{\pi^2}{k}R\right) - J'_m(kR)J_m\left(\frac{\pi^2}{k}R\right) = 0, \psi \tag{21}$$

which is the same as that obtained by Haugen and Tyvand in their analysis. Haugen and Tyvand found $m = 0$ to be the preferred convective mode for all R. Applying a Taylor series expansion of the determinant (19) with $m = 0$ yields terms of $O(\ln(R_w)/R_w)$, $O(1/R_w)$, $O(R_w)$ and higher order terms. The $O(\ln(R_w)/R_w)$-term is the one corresponding to Eq. (21). We now let k^0 be the wavenumbers obtained by Haugen and Tyvand, and k be the wavenumber obtained by us using a small value of R_w and use a Taylor series approach as in the insulated sidewalls case to balance the $O(1/R_w)$-term. We therefore apply $k = k^0 + O(1/\ln(R_w))$ and this choice of k implies that $\mathrm{Ra}_c = \mathrm{Ra}_c^0 + O(1/\ln(R_w))$, where Ra_c^0 are the critical Rayleigh numbers found by Haugen and Tyvand. Hence, our critical Rayleigh numbers will approach the Rayleigh numbers found by Haugen and Tyvand as $O(1/\ln(R_w))$ when R_w goes to zero, and we may consider the cylinder studied by Haugen and Tyvand as a special case of the annular cylinder case when the inner radius approaches zero.

Figure 8 shows the difference between the critical Rayleigh number for the circular cylindrical configuration of Ref. 13 and the present annular cylinder, with $R_w = 10^{-4}$. Despite the inner radius being very small, there remains a strong effect in terms of the critical Rayleigh number. However, the above analysis shows that this difference tends to zero as the inner radius shrinks further.

IV. NUMERICAL SIMULATIONS AND THE NONLINEAR REGIME

An unsteady 3D-solver which approximates the solution of the original nonlinear equations (1)–(3) has been written using pseudospectral methods in space and MATLAB's built-in package ODE15s in time. The solver finds the temperature distribution and velocity field for given values of R_w, R, and Ra. Therefore, it is possible to investigate how the nonlinear regime differs from that of the linearized system. The solver may also be used to examine the stability of existing convection cells: Through simulations, we may investigate the effect of variations in the Rayleigh number and find out how a specific convective mode responds when the domain changes or when a numerical perturbation is added during a simulation.

A. Pseudospectral discretization

Pseudospectral methods belong to the class of methods which approximate the unknown solution $u(x)$ by a sum of $(N+1)$ basis functions $\varphi_i(x)$ which span a finite subset of the full solution space,

$$u(x) \approx u_N(x) = \sum_{i=0}^{N} a_i \phi_i(x).$$

When solving the differential equation $Lu = f$, the goal of finite-dimensional function space representations is to choose the coefficients $\{a_i\}$ such that the residual defined by

$$R(x; a_0, a_1, \ldots, a_N) = Lu_N - f$$

is minimized in some appropriate sense. In contrast to variational type methods (wherein most finite element methods fall), pseudospectral methods constrain the solution space by setting the residual to zero in $(N+1)$ so-called collocation points $\{x_i\}$, that is,[16]

$$R(x_i; a_0, a_1, \ldots, a_N) = 0 \text{ for } i = 0, \ldots, N.\psi$$

The choice of collocation points is a critical aspect of the method. For linear differential operators, the above strategy leads to a linear system of equations which may be written in the form,

$$\mathbf{La} = \mathbf{b},\psi$$

where $\mathbf{L}$ is an $(N+1) \times (N+1)$ matrix with entries given by

$$a_{ij} = L\phi_j|_{x_i}.\psi$$

The $(N+1)$ –vector $\mathbf{b}$ has the entries

$$b_i = f(x_i),\psi$$

while the vector $\mathbf{a}$ consists of the unknown coefficients $\{a_i\}$. We use basis functions that are non-linear interpolating functions having value 1 at one collocation point and 0 at all the others, that is,

$$\phi_i(x_j) = \delta_{ij}.\psi$$

Hence, the coefficients $\{a_i\}$ are the function values of the approximated solution u_N in the nodes $\{x_i\}$. Each line in the matrix equation represents an equation for the function value in a specific node. Boundary conditions are handled by finding the matrix lines corresponding to which nodes the boundary conditions are applied and by substituting a discrete version of the boundary condition.

The grid points $\{x_i\}$ are selected with care in order to ensure that the numerical solution is of high accuracy. The optimal choice of grid points is dependent on the geometry of the domain. As we use cylindrical coordinates, we apply different choices of grid points for the radial, azimuthal, and vertical directions. The azimuthal direction is the finite interval $[0,2\pi]$ having the extra property of the solution being periodic. Here, the optimum choice is the Fourier nodes,[17] which are equally spaced in the angular coordinate given by

$$x_i = \frac{2\pi i}{N} \text{ for } i = 1, 2, \ldots, N.\psi$$

Both the radial and vertical direction are finite intervals ($[R_w$, $R]$ and $[0,1]$, respectively) without any periodicity. For these two intervals, the Chebyshev nodes are the optimum choice.[17] The Chebyshev nodes are given by

$$x_i = \cos\left(\frac{\pi i}{N}\right) \text{ for } i = 0, 1, \ldots, N$$

and these are easily shifted and scaled to fit into either of the two intervals.

When using spectral methods to discretize space, we expect the method to (potentially) converge as $O(1/N^N)$.[16,17] However, the full simulator is not expected to behave with this spectral accuracy since we have a time discretization which is also a source of error. For time discretization, we use MATLAB's ODE15s package which is an adaptive solver based on the backward differentiation formula.[18] ODE15s is designed for stiff differential algebraic problems, with adaptive 1st to 5th order accuracy.

B. Solution strategy

The governing equations (1)–(3) are solved by timestepping the Energy equation (3) and updating the velocity field using Darcy's Law (1) and the Mass equation (2) in each time step. For most cases, the steady-state solution $T = 1 - z$ is used as initial condition, hence letting the convective pattern appear due to numerical perturbations. Other initial conditions were used in the stability testing of the convective patterns: we then typically let convective modes from another stable setting or convective modes with an added numerical perturbation be given as the initial state. All solutions were timestepped until a steady-state solution was found. The criterion for obtaining a steady-state solution was that the temperature field could not change with values larger than 10^{-10} during the last 50 (non-dimensional) time units.

C. Results and discussion

The nonlinear code was tested for correctness by attempting to reproduce the critical Rayleigh numbers for some chosen values of R_w and R. Steady solutions were obtained for different values of Ra above the critical value given by linear theory. Weakly nonlinear theory for systems in which supercritical bifurcations occur indicates that the amplitude of convection is proportional to $(\mathrm{Ra} - \mathrm{Ra}_c)^{1/2}$, meaning that the square of the amplitude will be proportional to $(\mathrm{Ra} - \mathrm{Ra}_c)$. Thus, we may extrapolate backwards to determine the critical value of Ra from the point of view of the nonlinear code. In our context, the amplitude is given by

$$A = \sqrt{\left[\int_V \left(T \sin(m\theta) \mathrm{dV}\right]^2 + \left(\left[\int_V \left(T \cos(m\theta) \mathrm{dV}\right]^2\right)\right.\right.}\left.\left(\psi\right.\right.$$

where the integrals are taken over the volume of the annular cylinder. Values of Ra_c obtained in this way were compared with the analytical solutions and were found to compare well, thereby, lending confidence to the accuracy of the numerical coding and the quality of the numerical results.

Simulations of cases where the Rayleigh number is slightly supercritical generally gave the same convection pattern as the one given by linearized theory. The linear regime is, therefore, adequate for describing the convection pattern in the nonlinear regime for Rayleigh number slightly above the critical. However, when the linear analysis predicted p to be 4 or larger in the heat conducting sidewalls case, simulations always provided a smaller value of p. The reason is either that our solver is not able to reproduce convective modes with large values of p and heat conducting sidewalls

or that the linear analysis is not suitable for describing the nonlinear regime in these cases. When one is close to the boundary of two regions in the mode maps, the simulations may yield more than one possible state at onset, but the convective pattern always stabilized at the one predicted from the linear analysis.

Increasing the Rayleigh number provides several possible stable convection modes. A detailed comparison would have to be made with a weakly nonlinear analysis of the respective modes and their interaction, rather than with the linearized theory, and this aspect is outside of the scope of the present paper. However, Riley and Winters[19] made a very thorough study of the modal exchange mechanisms for convection in a two dimensional porous cavity using a stationary finite element solver coupled with bifurcation tracking software. In that paper, they showed that the second mode which appears is generally unstable but eventually gains stability as Ra increases at a bifurcation to a mixed mode. This scenario also applies in the present three-dimensional context, as may be seen in Figure 9. Here, we show a case with insulated sidewalls where $R_w = 0.1$ and $R = 0.7$. The critical Rayleigh numbers for the first two modes, (1, 0) and (2, 0), are 41.41 and 43.82. The (1,0)-mode remains stable with respect to numerical perturbations within the range of values of Ra we consider, but the (2,0)-mode is only stable above $\mathrm{Ra} = 50$. The second mode is unstable at lower Rayleigh numbers and disappears as the Rayleigh number decreases past its critical value; hence, the basic mode will take over as the sole stable mode when the secondary is in the process of disappearing since convection is still possible. Since the different modes have overlapping stability regions, several modes are sometimes possible for a given Rayleigh number. Therefore, we cannot speak of a *preferred* mode since the mode which appears depends on the initial conditions.

In the insulated sidewalls case, solutions which do not correspond to single linear modes were found. When the outer radius is greater than 1, stable mixed mode patterns could sometimes be found. For example, when $R_w = 0.7$ and $R = 2.1$, the first and second modes are the (5,0) and (2,1) modes. The critical Rayleigh numbers corresponding to these patterns are 39.51 and 39.58. When $\mathrm{Ra} = 39.75$, the steady stable solution shown in Figure 10 arises. It is clear from this figure that an $m = 2$ pattern dominates near the inner radius and an $m = 5$ pattern dominates near the outer radius; this would appear to be a stable mixed mode solution. Indeed, a physical reason why such a mixed mode should be stable is to appeal to the fact that the linear (5,0) and (2,1) modes are themselves concentrated towards the outer and inner radii, respectively, and this suggests that the presence of both modes in a stable nonlinear pattern is an example of optimizing the overall heat transport. The amplitude and stability regions for the pure (5,0) mode and the mixed mode are sketched for low Rayleigh numbers in Figure 11. This figure suggests that the mixed mode bifurcates away from the pure mode, rendering the latter unstable. The secondary mode (2,1) is unstable for all low Rayleigh numbers; hence, this mode is not present in the figure.

These mixed modes would be impossible to detect by the linear stability analysis, since the solution of the linearized equations only allow for one par of values of m and p to describe the convection in the whole domain. Hence, the mixed modes develop due to nonlinear effects and were observed when the difference between the outer and inner radius was larger than 1, possibly because of the severe clustering of modes present for these cylinders. We also observed that for increasing difference in radii, the mixed modes become more dominating over the basic mode; that is, the basic mode had a smaller stability region. It is likely to believe this effect to be even more important when the annular cylinder becomes wider; hence, the classical approach of assigning one value of m and p will not be sufficient to describe the convection patterns.

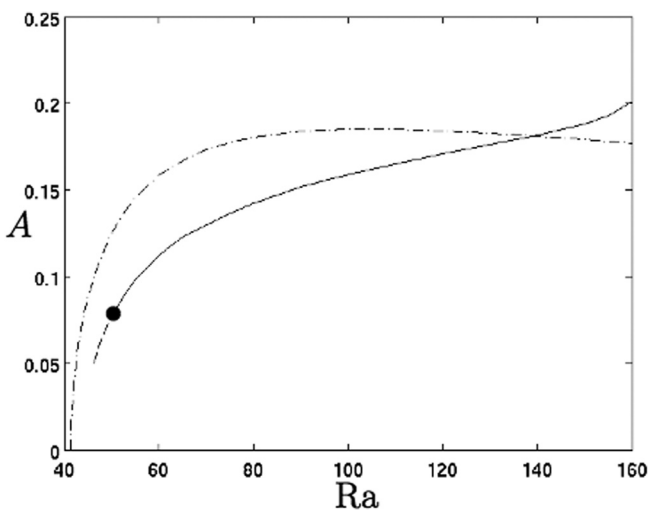

FIG. 9. The variation of the amplitude of convection with Rayleigh number for modes (1,0) and (2,0) for $R_w = 0.1$ and $R = 0.7$ and with insulated sidewalls. The dashed/dotted line is the amplitude of the basic mode (1,0). The continuous line is the amplitude of the stable part of the secondary mode (2,0) branch, while the dashed line is the unstable part.

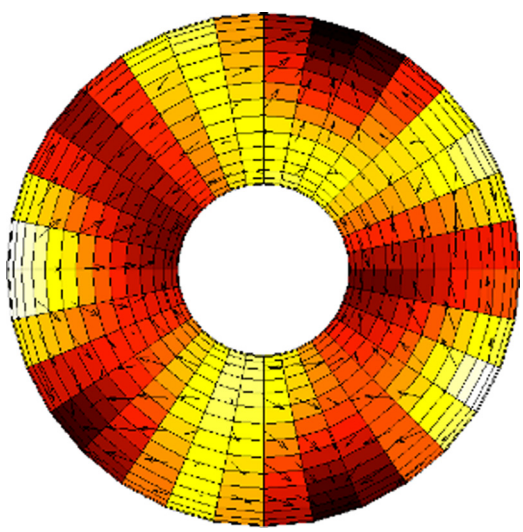

FIG. 10. (Color online) A stable mixed mode convection pattern corresponding to modes (5,0) and (2,1). The sidewalls are insulated while $R_w = 0.7$, $R = 2.1$, and $\mathrm{Ra} = 40$. The pattern displays $m = 2$ characteristics near the inner radius and $m = 5$ characteristics near the outer radius. The perceived value of p is either 0 or 1 depending on the chosen azimuthal position.

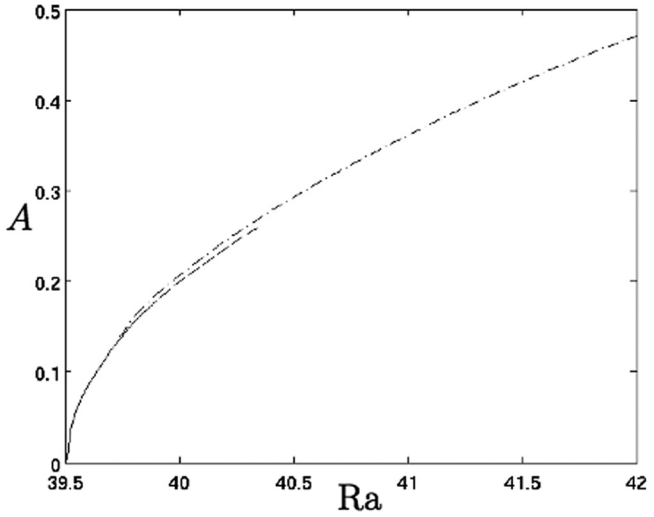

FIG. 11. The variation of the amplitude of convection with Ra for the case, $R_w = 0.7$ and $R = 2.1$, with insulated sidewalls. The continuous line corresponds to the stable part of basic mode (5,0) branch, which has the critical Rayleigh number 39.51, while the dashed line is the unstable region of this mode. The dashed/dotted line is the stable mixed mode branch.

We also note that, while mixed modes are usually unstable in the free convection context (see Riley and Winters,[19] for example), there are a few cases published where mixed modes may have stability. Examples may be found in the papers by Knobloch and Guckenheimer,[20] Kato and Fujimura,[21] and Borońska and Tuckerman.[22] This last case is of most relevance to the present paper because convection occurs within a cylindrical domain, and the authors show that there are a large number of stable nonlinear patterns which do not have simple counterparts in the corresponding linear theory.

We also tested for stability with respect to perturbations in the domain. Simulations with R_w and R close to bifurcation trajectories and the Rayleigh number over the critical (and under the secondary critical) always produced the anticipated convection mode, which then was stable with respect to numerical perturbations. Initializing the solver with a convection mode near a bifurcation trajectory, and perturbing the domain such that another convection mode should be the preferred according to the linear analysis, produced this other mode. Hence, the convection modes are not stable with respect to domain perturbations near the bifurcation trajectories. We may also conclude that the bifurcation trajectories are sharp; there are no transition zones. The mode at the other side of the trajectory will appear as a secondary mode, with stability properties as described above. The only exception was the appearance of mixed modes at onset; a mode intermediate of the two modes at each side of a bifurcation trajectory could be present at onset, but the convective pattern always stabilized at the anticipated mode when using low Rayleigh numbers.

V. CONCLUSION

For a porous medium filling a vertical, annular cylinder heated from below and having either conducting or insulated sidewalls, we have found critical Rayleigh numbers and preferred convective modes using linear stability analysis. In accordance with previous studies, we find that the critical Rayleigh numbers converge to $4\pi^2$ and always are larger for heat conducting sidewalls. The results show that the effect of an inner radius is more severe for heat conducting sidewalls. The presence of an inner radius increases the critical Rayleigh number significantly compared to the non-annular cylinder studied by Haugen and Tyvand.[13] For the insulated sidewalls, the inner radius does not have a similar effect. However, letting the inner radius approach zero, our results show that both the problems with conducting and insulated sidewalls degenerate into the ones studied by Haugen and Tyvand and by Zebib.[11]

The linear analysis provides maps over preferred convective modes for the two cases, and in general, the results show the appearance of more convection cells in radial direction for increasing outer radius and more convection cells in azimuthal direction for increasing the inner radius. For the insulated sidewalls case, we sometimes find other modes than Bau and Torrance[14] found in their paper. High-resolution simulations confirm our analysis.

Simulations with various inner and outer radii, and with Rayleigh numbers near critical, conform in most cases to the convection modes and critical Rayleigh numbers predicted from the linear analysis. The results show that the various modes have Rayleigh number dependent stability regimes, which is an important factor in predicting the convective mode occurring in practice. The nonlinear regime also reveals the appearance of mixed modes that are not represented in the basis of the linear analysis. As such, the numerical simulations both verify the linear stability analysis as well as give bounds on its validity.

[1]J. Bear, *Dynamics of Fluids in Porous Media* (Dover, New York, 1988).
[2]D. Ingham and I. Pop, *Transport Phenomena in Porous Media* (Elsevier Science, Oxford, 2005), Vol. 3.
[3]J. Bear and Y. Bachmat, *Introduction to Modelling Phenomena of Transport in Porous Media* (Kluwer Academic, Dordrecht, Netherlands, 1990).
[4]R. Freeze and J. Cherry, *Groundwater* (Prentice-Hall, Englewood Cliffs, NJ, 1979).
[5]C. W. Horton and F. T. Rogers, "Convection currents in a porous medium," J.Appl. Phys. **16**(6), 367 (2009).
[6]E. R. Lapwood, in *Mathematical Proceedings of the Cambridge Philosophical Society* (Cambridge University, Cambridge, England, 1948), Vol. 44, pp. 508–521.
[7]D. A. Nield, "Onset of thermohaline convection in a porous medium," Water Resour. Res. **4**(3), 553 (1968).
[8]D. A. Nield and A. Bejan, *Convection in Porous Media*, 3rd ed. (Springer, New York, 2006).
[9]J. L. Beck, "Convection in a box of porous material saturated with fluid," Phys. Fluids **15**(8), 1377 (1972).
[10]C. Y. Wang, "Onset of convection in a fluid-saturated rectangular box, bottom heated by constant flux," Phys. Fluids **11**(6), 1673 (1999).
[11]A. Zebib, "Onset of natural convection in a cylinder of water saturated porous media," Phys. Fluids **21**(4), 699 (1978).
[12]C. Y. Wang, "Thermo-convective stability of a fluid-saturated porous medium inside a cylindrical enclosure: Permeable top constant flux heating," Mech. Res. Commun. **26**(5), 603 (1999).
[13]K. B. Haugen and P. A. Tyvand, "Onset of thermal convection in a vertical porous cylinder with conducting wall," Phys. Fluids **15**(9), 2661 (2003).
[14]H. H. Bau and K. E. Torrance, "Onset of convection in a permeable medium between vertical coaxial cylinders," Phys. Fluids **24**(3), 382 (1981).
[15]D. A. S. Rees and P. A. Tyvand, "The Helmholtz equation for convection in two-dimensional porous cavities with conducting boundaries," J. Eng. Math. **49**(2), 181 (2004).

[16]J. P. Boyd, *Chebyshev and Fourier Spectral Methods* (Dover, New York, 2001).
[17]L. N. Trefethen, *Spectral Methods in MATLAB* (Society for Industrial and Applied Mathematics, Philadelphia, 2000).
[18]M. W. Reichelt and L. F. Shampine, "The MATLAB ode suite," SIAM J. Sci. Comput. (USA) **18**(1), 1 (1997).
[19]D. S. Riley and K. H. Winters, "Modal exchange mechanisms in Lapwood convection," J. Fluid Mech. **204**, 325 (1989).
[20]E. Knobloch and J. Guckenheimer, "Convective transitions induced by a varying aspect ratio," Phys. Rev. A **27**(1), 408 (1983).
[21]Y. Kato and K. Fujimura, "Prediction of pattern selection due to an interaction between longitudinal rolls and transverse modes in a flow through a rectangular channel heated from below," Phys. Rev. E **62**(1), 601 (2000).
[22]K. Borońska and L. Tuckerman, "Extreme multiplicity in cylindrical Rayleigh-Bénard convection. II. Bifurcation diagram and symmetry classification," Phys. Rev. E **81**(3), 036321 (2010).